Rational Redesign of the 4-Chlorobenzoate Binding Site of 4-Chlorobenzoate: Coenzyme A Ligase for Expanded Substrate Range[†,‡,§]

Rui Wu,[||,⊥] Albert S. Reger,[⊥,@] Jian Cao,[||] Andrew M. Gulick,*[,@] and Debra Dunaway-Mariano*[,||]

Department of Chemistry, University of New Mexico, Albuquerque, New Mexico 87131, and Hautpman-Woodward Medical Research Institute and Department of Structural Biology, State University of New York at Buffalo, Buffalo, New York 14214

Received August 9, 2007; Revised Manuscript Received September 26, 2007

ABSTRACT: Environmental aromatic acids are transformed to chemical energy in bacteria that possess the requisite secondary pathways. Some of these pathways rely on the activation of the aromatic acid by coenzyme A (CoA) thioesterification catalyzed by an aromatic acid: CoA ligase. Adaptation of such pathways to the bioremediation of man-made pollutants such as polychlorinated biphenyl (PCB) and dichlorodiphenyltrichloroethane (DDT) requires that the chlorinated benzoic acid byproduct that is formed be able to be eliminated by further degradation. To take advantage of natural benzoic acid degrading pathways requiring initial ring activation by thioesterification, the pathway aromatic acid:CoA ligase must be an effective catalyst with the chlorinated benzoic acid. This study, which focuses on the 4-chlorobenzoate:CoA ligase (CBL) of the 4-monochlorobiphenyl degrading bacterium *Alcaligenes* sp. strain ALP83, was carried out to determine if the 4-chlorobenzoate binding site of this enzyme can be transformed by rational design to recognize the chlorobenzoic acids formed in the course of breakdown of other environmental PCB congeners. The fundamental question addressed in this study is whether it is possible to add or subtract space from the substrate-binding pocket of this ligase (to complement the topology of the unnatural aromatic substrate) without causing disruption of the ligase catalytic machinery. Herein, we report the results of a substrate specificity analysis that, when interpreted within the context of the X-ray crystal structures, set the stage for the rational design of the ligase for thioesterification of two PCB-derived chlorobenzoic acids. The ligase was first optimized to catalyze CoA thioesterification of 3,4-dichlorobenzoic acid, a poor substrate, by truncating Ile303, a large hydrophobic residue that packs against the ring *meta*-C(H) group. The structural basis for the ∼100-fold enhancement in the rate of 3,4-dichlorobenzoate thioesterification catalyzed by the I303A and I303G CBL mutants was validated by determination of the crystal structure of the 3,4-dichlorobenzoate-bound enzymes. Determinations of the structures of I303 mutant complexes of 3-chlorobenzoate, a very poor substrate, revealed nonproductive binding as a result of the inability of the substrate ring C(4)H group to fill the pocket that binds the C(4)Cl group of the native substrate. The C(4)Cl pocket of the CBL I303A mutant was then reduced in size by strategic amino acid replacement. A 54-fold improvement in catalytic efficiency was observed for the CBL F184W/I303A/V209T triple mutant. The results of this investigation are interpreted as evidence that the plasticity of the ligase catalytic scaffold is sufficient to allow expansion of substrate range by rational design. The combination of structural and kinetic analyses of the constructed mutants proved to be an effective approach to engineering the ligase for novel substrates.

Chlorinated aromatics, exemplified by polychlorinated biphenyls (PCBs)[1] and dichlorodiphenyltrichloroethane (DDT), have accumulated in the environment as a result of global dispersion (*1*−*3*). Research into methods applicable to the removal of PCB and DDT contaminants from the environment has been stimulated by the demonstration of their toxic, carcinogenic, and teratogenic properties (*4*−*7*). One effective strategy is "bioremediation", a process that employs the chemical pathways of naturally occurring bacteria, or bacteria that have been genetically engineered, for in vivo degradation (*8*−*11*).

PCBs are chlorinated analogues of biphenyl. Biphenyl is oxidatively degraded by specialized soil-dwelling bacteria to benzoate and 2-hydroxypenta-2,4-dienoate (*12*−*17*). These two products are further oxidized to metabolites that are degraded by the citric acid cycle. PCB congeners that are

[†] This work was supported by NIH Grant GM28688 to D.D.-M. and by NIH Grant GM-068440 to A.M.G. Protein structure determinations were carried out at the Cornell High Energy Synchrotron Source (CHESS) which is supported by the National Science Foundation under Grant DMR 0225180 and the National Institutes of Health through its National Center for Research Resources under Grant 5 P41 RR001646-23.

[‡] R.W., J.C., and D.D.-M. contributed the biochemical studies, and A.S.R. and A.M.G. contributed the X-ray structure analyses.

[§] The atomic coordinates and structure factors for four structures have been deposited with the Protein Data Bank: 4-chlorobenzoate:CoA ligase I303A bound to 3-chlorobenzoate (2QVZ) and to 3,4-dichlorobenzoate (2QWO) and 4-chlorobenzoate:CoA ligase I303G bound to 3-chlorobenzoate (2QVX) and 3,4-dichlorobenzoate (2QVY).

* To whom correspondence should be addressed. D.D.-M. (for information regarding the kinetic studies): Department of Chemistry and Chemical Biology, University of New Mexico, Albuquerque, NM 81713; telephone, (505) 277-3383; fax, (505) 277-6202; e-mail, dd39@unm.edu. A.M.G. (for information regarding the structure determinations): Hauptman-Woodward Medical Research Institute and Department of Structural Biology, State University of New York at Buffalo, Buffalo, NY 14214; telephone, (716) 898-8619; fax, (716) 898-8660; e-mail, gulick@hwi.buffalo.edu.

[||] University of New Mexico.

[⊥] These authors share first authorship.

[@] State University of New York at Buffalo.

[1] Abbreviations: PCBs, polychlorinated biphenyls; DDT, dichlorodiphenyltrichloroethane; CoA, coenzyme A; CBL, 4-chlorobenzoate:CoA ligase; 4-CB-AMP, 4-chlorobenzoyladenosine 5′-monophosphate; PP_i, inorganic pyrophosphate; AMP, adenosine 5-monophosphate; NADH, β-nicotinamide adenine dinucleotide; PEP, phosphoenolpyruvate; PA, phenylacetate; 4-CB, 4-chlorobenzoate; 3-CB, 3-chlorobenzoate; 3,4-DCB, 3,4-dichlorobenzoate; DTT, dithiothreitol; K^+Hepes, potassium salt of *N*-(2-hydroxyethyl)piperzine-*N*′-2-ethanesulfonate; SDS−PAGE, sodium dodecyl sulfate−polyacrylamide gel electrophoresis.

10.1021/bi701609w CCC: $37.00
Published on Web 11/21/2007

Scheme 1: 4-Chlorobenzoate Dehalogenation Pathway

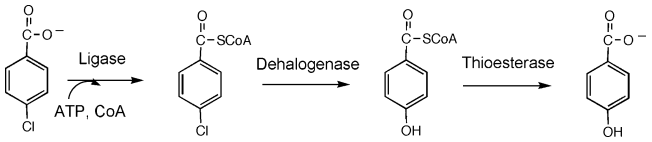

chlorinated at only one of the two aromatic rings are converted to 2-hydroxypenta-2,4-dienoate and chlorinated benzoate (*10*). If not degraded, the chlorinated benzoate byproduct accumulates and inhibits bacterial growth (*10*). Thus, to be effective at the bioremediation of a PCB, the bacterium must couple the biphenyl pathway with a chlorobenzoate-degrading pathway. Such a strategy has been observed to operate in the natural 4-monochlorobiphenyl degrader *Alcaligenes* sp. strain ALP83 (*18*, *19*). This strain was isolated from PCB-contaminated soil and shown to degrade 4-monochlorobiphenyl to carbon dioxide by using the 4-chlorobenzoate dehalogenation pathway in combination with the biphenyl oxidation pathway (Scheme 1) (*20*, *21*). The conversion of the 4-chlorobenzoate to the metabolite 4-hydroxybenzoate transforms the growth inhibitor to an additional source of chemical energy.

The 4-chlorobenzoate is activated for hydrolytic dehalogenation by conversion to the corresponding CoA thioester (*22*). CoA thioesterification of the aromatic carboxylate group is a strategy used in other bacterial secondary pathways that degrade aromatic rings to metabolites, as exemplified by the phenylacetate (*23*), benzoate (*24*), and reductive 4-hydroxybenzoate (*25*) catabolic pathways. These pathways serve as valuable starting points for the engineering of novel pathways for use in bioremediation of man-made aromatic pollutants. The mono-, di-, and trichlorinated benzoates generated from microbial degradation of asymmetric PCBs, for example, might be mineralized by using designer pathways that employ engineered enzymes. The aromatic acid:CoA ligase catalyzes the first step of the pathway, and therefore, it is the logical starting point for engineering the pathway enzymes for degradation of a novel substrate.

The bacterial ligases that catalyze the transformation of the aromatic acid to the corresponding CoA thioester are not well-characterized in part because of their instability and/or poor expression of their encoding gene in *Escherichia coli*.[2] The 4-chlorobenzoate:CoA ligase (CBL), however, is an exception (*26*). The recently reported X-ray structure of *Alcaligenes* sp. strain ALP83 CBL complexed with 4-chlorobenzoate (*27*) opened the door to the expansion of substrate range by rational design of the 4-chlorobenzoate binding site. Rational design alone, or in combination with saturation mutagenesis, has been successfully used in the modification of enzyme specificity (for recent examples, see refs *28*−*35*).

The first phase of the work, reported herein, focused on the analysis of the substrate specificity of CBL within the context of the structure of the 4-chlorobenzoate binding site. 3,4-Dichlorobenzoate and 3-chlorobenzoate were selected as substrates for the second phase of our work, which concentrated on the restructuring of the 4-chlorobenzoate binding pocket by strategic amino acid replacement. The results reported below show that the substrate range of CBL is subject to extension through structure-guided protein engineering. The plasticity of the binding site, which tolerates these structural changes, is no doubt a key component of the natural evolution of the acyl adenylate-forming enzyme superfamily (to which CBL belongs) (*22*), allowing continual diversification within the family to reach novel organic acid metabolites.

[2] There are few reports in the literature of the characterization of purified aromatic acid ligases in general and recombinant aromatic ligases in particular. In our hands, the yield of recombinant 4-chlorobenzoate:CoA ligase derived from 4-chlorobenzoate-degrading *Pseudomonas* and *Arthrobacter* strains using *E. coli* clones as the overexpression system is low and the activity of the purified ligase is unstable. We have met with limited or no success in the isolation of active recombinant bacterial phenylacetate:CoA ligase, benzoate:CoA ligase, or aminobenzoate:CoA ligase. The reason(s) for this undesirable behavior is not clear.

MATERIALS AND METHODS

Materials. Except where mentioned, all chemicals and coupling enzymes [adenylate kinase (EC 2.7.4.3), pyruvate kinase (EC 2.7.1.40), and lactate dehydrogenase (EC 1.1.1.27)] were purchased from Sigma-Aldrich. Custom-synthesized PCR primers were obtained from Invitrogen, as were the restriction enzymes, the *pfu* polymerase, and the T4 DNA ligase. Competent JM109 and BL21(DE3) cells were purchased from Stratagene, and the pQE-70 vector was purchased from QIAGEN. DNA sequencing analysis was carried out by the DNA Sequencing Facility of the University of New Mexico. SDS−PAGE was performed with gels prepared from a 12% acrylamide gel with a 3% stacking gel (37.5:1 acrylamide:biacryamide ratio) (Bio-Rad).

CBL Preparation. A single colony of *E. coli* JM109 containing the plasmid *Sph*I-*Bgl*II-pQE-70-CBAL (*20*, *21*) was used to inoculate 10 mL of LB medium containing 50 μg/mL ampicillin at 37 °C with mixing at 250 rpm. The 10 mL culture was then used to inoculate 10 L of fresh LB medium containing 50 μg/mL ampicillin, and the culture was grown at 20 °C with mixing at 200 rpm. After 26 h (OD $\sim$ 0.7 at 600 nm), isopropyl β-thiogalactopyranoside was added to a final concentration of 1 mM. Following incubation at 20 °C and mixing at 200 rpm for 10 h, the cells were harvested by centrifugation at 5000*g* for 15 min. The 10 g pellet was suspended in 100 mL of lysis buffer [50 mM NaH_2PO_4 (pH 8.0), 10 mM imidazole, and 1 mM DTT] containing 10 μL of 0.1 mM protease inhibitor PMSF, passed through a French press at 1200 psi, and then centrifuged at 48000*g* and 4 °C for 30 min. The supernatant was loaded onto a Ni-NTA agarose column (QIAGEN, 25 mL), which had been pre-equilibrated with the lysis buffer. The column was washed with 500 mL of wash buffer [50 mM NaH_2PO_4 (pH 8.0), 50 mM imidazole, and 1 mM DTT] and then eluted with 200 mL of elution buffer [50 mM NaH_2PO_4, 250 mM imidazole, and 1 mM DTT (pH 8.0)]. The fractions were analyzed by SDS−PAGE and then selectively pooled and dialyzed for 3 h against three changes of 1.5 L of 50 mM K^+Hepes buffer containing 1 mM DTT (pH 7.5 and 25 °C). The protein purity was verified by SDS−PAGE analysis. The protein concentration was determined by using the Bradford method (*36*) and by measuring the absorbance at 280 nm (ϵ = 27 760 M^{-1} cm^{-1}). The yield was 6 mg/g of wet cells.

CBL Activity Assays. (1) Direct Continuous Assay. The CBL reaction with 4-chlorobenzoate was assessed at 25 °C by measuring the increase in the absorbance of the 1 mL

reaction solution at 300 nm ($\Delta\epsilon = 2.5$ mM^{-1} cm^{-1}). The 1 mL assay solution contained 2 mM 4-chlorobenzoate, 1 mM CoA, 3.5 mM ATP, and 15 mM $MgCl_2$ in 50 mM K^+Hepes (pH 7.5).

(2) Coupled Assay. The CBL reactions with the various carboxylate substrates were monitored by using the coupled assay that detects the formation of AMP through the sequential activities of adenylate kinase, pyruvate kinase, and lactate dehydrogenase. The 1 mL solutions initially contained 1 mM CoA, 3.5 mM ATP, 15 mM $MgCl_2$, 200 μM NADH, 3 mM PEP, 5 mM KCl, 11 units of adenylate kinase (EC 2.7.4.3), 9 units of pyruvate kinase (EC 2.7.1.40), and 9 units of lactate dehydrogenase (EC 1.1.1.27) in 50 mM K^+Hepes (pH 7.5 and 25 °C). The decrease in absorbance at 340 nm due to the oxidation of two molecules of NADH per molecule of AMP formed was monitored.

Determination of Steady-State Kinetic Constants. The initial velocity for CBL-catalyzed reactions was measured as a function of one substrate concentration (varied between 0.5- and 5-fold K_M) with the two cosubstrates at a fixed, saturating concentration (1 mM CoA, 3.5 mM ATP, and 2 mM 4-chlorobenzoate). The concentration of $MgCl_2$ used for each reaction solution is 11.5 mM plus the millimolar concentration of the ATP present. Reaction solutions were buffered with 50 mM K^+Hepes (pH 7.5 and 25 °C). The V_{max} and K_M values were calculated from the initial velocity data using eq 1 and KinetAsyst. The k_{cat} was calculated from the ratio of V_{max} and enzyme concentration.

$$V = V_{max}[S]/([S] + K_M) \quad (1)$$

where V is the initial velocity, V_{max} the maximum velocity, [S] the varied substrate concentration, and K_M the Michaelis constant.

Mutant CBL Preparation. The CBL mutant genes were prepared by using a PCR-based method that employed *Alcaligenes* sp. strain ALP83 (NCBI accession number AF 537222.1) derived SphI-BglII-pQE-70-CBAL subclone (*20*, *21*) as the template, and commercial primers. The purified PCR product was digested with SphI and BglII (Invitrogen) and ligated to the SphI- and BglII-digested plasmid pQE-70 [which includes the six-His tag and stop codon (QIAGEN)] with T4 DNA ligase (Invitrogen). The mutant gene sequence was verified by DNA sequencing which was carried out by the Center for Genetics in Medicine, University of New Mexico. The mutant proteins were prepared using the same procedure that was used in the preparation of recombinant wild-type CBL (see above). The homogeneity of each purified mutant CBL was demonstrated by SDS−PAGE analysis.

Crystallization and Determination of Structures of CBL Ile303 Mutants. The Ile303 CBL mutant proteins were crystallized by hanging drop vapor diffusion using a precipitant consisting 14−22% pentaerythritol propoxylate 426 (*37*) and 50 mM 1,3-bis[tris(hydroxymethyl)methylamino]-propane (pH 6.5−6.75). The alanine and glycine mutants were each cocrystallized in the presence of ATP and either 3-chlorobenzoate or 3,4-dichlorobenzoate. Crystals were grown at 4 °C and appeared within 1−2 days. Crystals were cryoprotected by being transferred sequentially to solutions containing 4−24% ethylene glycol, then mounted in a nylon cryoloop, and cryo-cooled in liquid nitrogen. The final cryoprotectant solution contained 24% ethylene glycol, 24% pentaerythritol propoxylate 426, and 50 mM 1,3-bis[tris-(hydroxymethyl)methylamino]propane (pH 6.75). Additionally, all cryoprotectant solutions contained 1 mM ATP and 3-chlorobenzoate or 3,4-dichlorobenzoate.

Data were collected for crystals of the Ile303 CBAL mutants at beamline F2 of the Cornell High Energy Synchrotron Source. Data collection was performed with an ADSC Quantum-210 detector set at a crystal−detector distance of 240 mm using X-rays at a wavelength of 0.97930 Å. Data were indexed, integrated, and scaled with HKL2000 (*38*). Despite the difference in the solution pH prevailing under the crystallization conditions, the crystals were isomorphous to the wild-type crystals used previously (*27*); however, the unit cells were longer by ∼2.5%. Because of this increase in the lengths of cell axes, the structures were determined by molecular replacement using MOLREP (*39*).

The search model used was the SeMet-containing structure (PDB entry 1T5H). To generate the search model, the SeMet residues were replaced with methionines, the water molecules and metal ions were removed, and the Ile303 was replaced with the alanine or glycine side chain. In all cases, the solution was the top peak of the rotation and translation searches. The molecular replacement solution was subjected to a round of refinement with REFMAC5 (*40*) followed by continued cycles of manual model building with COOT (*41*) and maximum likelihood refinement. Weighted individual *B*-factors were applied for all models. Near completion of the modeling, TLS refinement (*42*) was used to apply grouped anisotropic thermal parameters to the N- and C-terminal domains, which resulted in a drop in R_{free}. Electron densities for the 3-chlorobenzoate and 3,4-dichlorobenzoate ligands were clear, and their atoms were added after several rounds of model building and refinement. Given the limited resolution, water molecules were conservatively added to spherical, or nearly spherical, density that was present in the difference maps at $>2.5\sigma$. Although ATP had been included in the crystallization media, no density for the nucleotide was apparent in any of the structures.

Atomic coordinates and structure factors for all four structures have been deposited in the Protein Data Bank: 2QVZ for I303A bound to 3-CB, 2QWO for I303A bound to 3,4-DCB, 2QVX for I303G bound to 3-CB, and 2QVY for I303G bound to 3,4-DCB.

RESULTS AND DISCUSSION

Structural Basis for Recognition of the CBL−4-Chlorobenzoate Complex. The 4-chlorobenzoate binding pocket residues Phe184, His207, Phe249, Ala280, Ile303, Gly305, Met310, and Asn311 (Figure 1) are conserved among the six additional known CBL sequences from *Comamonas*, *Pseudomonas*, and *Arthrobacter* species (divergence to 62% nonidentity between sequence pairs). Binding pocket residues Val208 (Thr in *Pseudomonas* CBL) and Val209 (Ile in *Arthrobacter* CBL), on the other hand, are not stringently conserved. The 4-chlorobenzoate aromatic ring and its C(4) chloro substituent are surrounded by the side chains of the nonpolar pocket residues, and by the methylene group of the Asn311 side chain. The structure of unliganded CBL (determined previously at 2.0 Å resolution) shows three solvent molecules present in the 4-chlorobenzoate binding

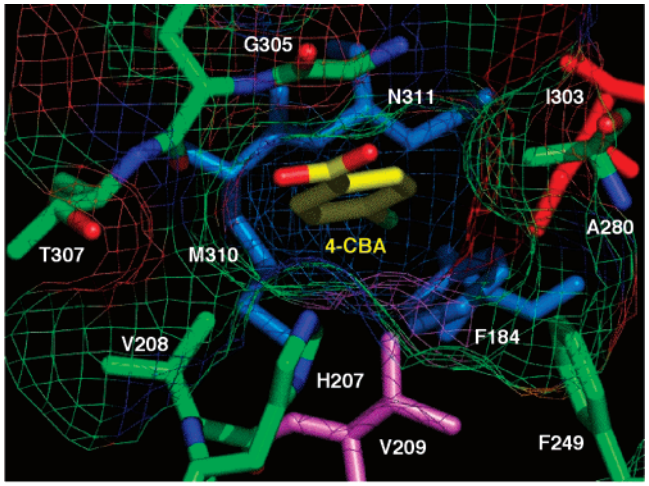

FIGURE 1: Representation of the 4-chlorobenzoate binding pocket in CBL from *Alcaligenes* sp. strain ALP83. This figure was generated from the X-ray coordinates of wild-type CBL in complex with 4-chlorobenzoate (PDB entry 1T5D) (*27*) using Pymol (*52*). The 4-chlorobenzoate ligand is shown with yellow carbon atoms, red oxygen atoms, and a green chlorine atom.

pocket (*27*). When the ligand binds, the solvent water molecules are displaced. The short distance (4 Å on average) separating the 4-chlorobenzoate ring carbon atoms and the binding pocket residues allows for van der Waals interaction. The ring carboxylate projects outside the entrance of the hydrophobic binding pocket and is positioned 3.7 Å from the His207 imidazole Nτ (Figure 1). This distance is outside of the distance for strong hydrogen bond formation. Thus, unless the distance is decreased by a change in conformation induced by MgATP binding, it may be assumed that the orientation of the ring carboxylate is dictated by the confinement of the aromatic ring within the hydrophobic binding pocket. As this work progressed, we discovered that the hydrophobic binding pocket does in fact play an essential role in productive binding (see the discussion of the 3-chlorobenzoate−CBL I303A and I303G complexes).

On the basis of the structure of the 4-chlorobenzoate binding site, we anticipated a narrow substrate range. To define this range, the steady-state kinetic constants for CBL-catalyzed thioesterification of a series of organic acids were measured, with particular emphasis placed on ring-substituted benzoates. The two cosubstrates ATP and CoA, and the cofactor Mg^{2+}, were present in the reaction solutions at saturating concentrations (see Table 1). Under these conditions, the 4-chlorobenzoate $k_{cat} = 9.2\ s^{-1}$, $K_M = 0.93\ \mu M$, and $k_{cat}/K_M = 9.9 \times 10^6\ M^{-1}\ s^{-1}$. With phenylacetate serving as the substrate, the k_{cat} value is reduced 3 orders of magnitude and the k_{cat}/K_M value is reduced 6 orders of magnitude (Table 1). The methylene group increases the distance between the aromatic ring and the carboxylate group, which in turn reduces substrate binding affinity and hinders the orientation of the substrate for reaction with the ATP. The k_{cat} measured for hexanoate thioesterification is ~5-fold lower than that measured for 4-chlorobenzoate thioesterification, and the hexanoate k_{cat}/K_M is $\sim 1 \times 10^4$-fold lower. These results suggest that the CBL active site can accommodate the flexible, hydrophobic hexanoyl unit, however at a substantial cost to binding affinity and turnover rate. On the basis of these results, we conclude that CBL has evolved to target a benzoate substrate, which from the location of its encoding gene within the 4-chlorobenzoate dehalogenation pathway operon (*20*, *22*), we know to be 4-chlorobenzoate. CBL is thus functionally distinct from the acyl-CoA synthetases of primary metabolism and the phenylacetate:CoA ligase of the phenylacetate catabolic pathway.

The determination of the substrate specificity toward ring-substituted benzoates defines the spatial and electrostatic requirements for the active site and sets the stage for the engineering of this enzyme to accept alternate benzoate substrates. Comparison of the substrate activities of the various *para*-substituted (C4), *ortho*-substituted (C2 or C6), and *meta*-substituted (C3 or C5) benzoates reveals that CBL catalyzes the thioesterification of a wide range of *para*-substituted benzoates with varying degrees of efficiency and that CBL displays very low activity with the *ortho*- and *meta*-substituted benzoates (Table 1). These observations can be rationalized within the context of the structure of the 4-chlorobenzoate binding site (Figure 1). Specifically, the C(4)Cl group of the bound 4-chlorobenzoate is accommodated by a small hydrophobic binding pocket [hereafter termed the "C(4)X pocket"] formed by Cγ and Cϵ of the Met310 side chain, Cβ of the Asn311 side chain, and the aromatic ring of Phe184. Substrate discrimination of *para*-substituted benzoates is therefore based on the compatibility of the size, shape, and polarity of the benzoate C(4) substituent with the C(4)X pocket. Notably, benzoate itself is a poor substrate. We assume that because of its small size, the hydrogen atom at C(4) does not fill the C(4)X pocket, and consequently, ligand binding affinity and orientation are adversely affected. The majority of the *para*-substituted benzoates that were tested, however, proved to be efficient CBL substrates ($k_{cat}/K_M > 10^4\ s^{-1}\ M^{-1}$). Among these are the *para*-halosubstituted benzoates 4-fluorobenzoate, 4-bromobenzoate, and 4-iodobenzoate. Remarkably, the electron induction provided by the C(4)F group does not appear to strongly impair the reactivity of the ring carboxylate, nor does the desolvation of the C(4)F group into the hydrophobic pocket prevent binding. Indeed, the k_{cat}/K_M of 4-fluorobenzoate, although 50-fold smaller than the k_{cat}/K_M measured for 4-chlorobenzoate, is 10-folder greater than the k_{cat}/K_M measured for benzoate.

CBL also shows significant activity with 4-nitrobenzoate, 4-methylbenzoate, 4-ethylbenzoate, 4-methoxybenzoate, 4-cyanobenzoate, and 4-trifluoromethylbenzoate. In contrast, the k_{cat}/K_M of 4-hydroxybenzoate is ~10000-fold smaller than that of 4-chlorobenzoate. This reduction may be attributed to the strong hydrogen bonding properties of the C(4)OH group. Specifically, the loss of the three H-bonds between the C(4)OH group and water that will occur upon complex formation is likely to reduce the binding affinity. Moreover, despite the comparatively high nucleophilicity of the 4-hydroxybenzoate carboxylate (because of donation of electrons from the ring hydroxyl group), the k_{cat} is also diminished. Because 4-hydroxybenzoate is the end product of the 4-chlorobenzoate dehalogenation pathway (Scheme 1) (*22*), it is essential that CBL discriminate between it and 4-chlorobenzoate. Clearly, the evolution of CBL has optimized its reactivity with 4-chlorobenzoate while minimizing its reactivity with 4-hydroxybenzoate.

Examination of the steady-state kinetic constants for the *ortho*- and *meta*-substituted benzoate substrates reveals that

Table 1: Steady-State Kinetic Constants for CBL-Catalyzed Thioesterification of 4-Chlorobenzoate Analogues in 50 mM K^+Hepes (25 °C and pH 7.5) Containing 1 mM CoA, 3.5 mM ATP, and 15 mM $MgCl_2$[a]

substrate	k_{cat} (s^{-1})	K_M (μM)	k_{cat}/K_M (s^{-1} M^{-1})
phenylacetate	$(1.9 \pm 0.1) \times 10^{-3}$	$(1.8 \pm 0.1) \times 10^{3}$	1.1
hexanoate	1.9 ± 0.1	$(6.3 \pm 0.5) \times 10^{3}$	3.1×10^{2}
4-chlorobenzoate	9.2 ± 0.2	$(9.3 \pm 0.9) \times 10^{-1}$	9.9×10^{6}
benzoate	7.5 ± 0.2	$(4.1 \pm 0.3) \times 10^{2}$	1.8×10^{4}
4-fluorobenzoate	$(1.01 \pm 0.03) \times 10$	$(4.2 \pm 0.4) \times 10$	2.4×10^{5}
4-bromobenzoate	7.0 ± 0.4	1.1 ± 0.2	6.3×10^{6}
4-hydroxybenzoate	$(9.9 \pm 0.1) \times 10^{-1}$	$(1.50 \pm 0.04) \times 10^{3}$	6.6×10^{2}
4-nitrobenzoate	3.4 ± 0.1	$(1.8 \pm 0.2) \times 10^{2}$	1.9×10^{4}
4-methylbenzoate	6.6 ± 0.2	$(1.8 \pm 0.1) \times 10$	3.7×10^{5}
4-ethylbenzoate	3.2 ± 0.1	$(1.1 \pm 0.1) \times 10^{2}$	2.9×10^{4}
4-iodobenzoate	3.82 ± 0.05	2.3 ± 0.1	1.7×10^{6}
4-methoxybenzoate	4.6 ± 0.1	$(2.0 \pm 0.2) \times 10^{2}$	2.3×10^{4}
4-cyanobenzoate	2.90 ± 0.06	$(9.0 \pm 0.6) \times 10$	3.2×10^{4}
4-trifluoromethylbenzoate	3.6 ± 0.1	$(3.4 \pm 0.4) \times 10^{2}$	1.1×10^{4}
2-chlorobenzoate	6.9 ± 0.1	$(3.4 \pm 0.2) \times 10^{2}$	2.0×10^{4}
3-chlorobenzoate	$(1.40 \pm 0.02) \times 10^{-1}$	$(8.0 \pm 0.5) \times 10^{2}$	1.7×10^{2}
3,4-dichlorobenzoate	$(9.3 \pm 0.1) \times 10^{-1}$	$(4.6 \pm 0.1) \times 10^{2}$	2.0×10^{3}
2,4-dichlorobenzoate	$(5.13 \pm 0.09) \times 10^{-2}$	$(1.49 \pm 0.09) \times 10^{2}$	3.4×10^{2}
2-bromobenzoate	$(2.76 \pm 0.08) \times 10^{-2}$	$(1.8 \pm 0.1) \times 10^{3}$	1.5×10
3-bromobenzoate	$(1.47 \pm 0.02) \times 10^{-2}$	$(2.6 \pm 0.1) \times 10^{2}$	5.7×10
3-hydoxybenzoate	$(2.1 \pm 0.1) \times 10^{-1}$	$(2.4 \pm 0.4) \times 10^{3}$	8.9×10
3-methylbenzoate	$(4.2 \pm 0.2) \times 10^{-1}$	$(6.0 \pm 0.5) \times 10^{3}$	7.0×10
3-methoxybenzoate	$(7.2 \pm 0.7) \times 10^{-1}$	$(5.3 \pm 0.9) \times 10^{3}$	1.4×10^{2}
2-methylbenzoate	$(4.1 \pm 0.2) \times 10^{-1}$	$(1.05 \pm 0.09) \times 10^{4}$	3.9×10
2-cyanobenzoate	$<1.7 \times 10^{-4}$		
3-cyanobenzoate	$<4.2 \times 10^{-4}$		
3-nitrobenzoate	$<1.0 \times 10^{-4}$		
2-iodobenzoate	$<5.5 \times 10^{-4}$		
3-iodobenzoate	$<1.4 \times 10^{-3}$		
2-methoxybenzoate	$<8.2 \times 10^{-4}$		
2,5-dichlorobenzoate	$<8.6 \times 10^{-4}$		
2,6-dichlorobenzoate	$<1.7 \times 10^{-4}$		
2,3,5-trichlorobenzoate	$<6.0 \times 10^{-4}$		

[a] See Materials and Methods for details. Error limits are derived from the data fitting and not from replicate measurements.

K_M is dramatically increased[3] and k_{cat} is dramatically decreased. The *meta*-substituted benzoates 3-chlorobenzoate, 3-bromobenzoate, 3-hydroxybenzoate, 3-methylbenzoate, and 3-methoxybenzoate are especially poor substrates as are the *ortho*-substituted benzoates 2-bromobenzoate and 2-methylbenzoate. The 2-chlorobenzoate shows a modest level of activity: $k_{cat}/K_M = 2 \times 10^4$ M^{-1} s^{-1} which is 500-fold lower than the 4-chlorobenzoate k_{cat}/K_M value. Given that the differences in size and electronic properties of Cl versus Br are small, it is curious that the k_{cat}/K_M value measured for the 2-bromobenzoate is 3 orders of magnitude lower than the 4-chlorobenzoate k_{cat}/K_M value. 2-Cyano-, 2-iodo-, 3-cyano-, 3-nitro-, 3-iodo-, 2-methoxy-, 2,5-dichloro-, 2,6-dichloro-, and 2,3,5-trichlorobenzoate are not substrates for CBL.

Notably, the first target for the engineering, 3,4-dichlorobenzoate, displays a modest level of activity ($k_{cat}/K_M = 2 \times 10^3$ M^{-1} s^{-1}). The second target, 3-chlorobenzoate, is much less active ($k_{cat}/K_M = 1.7 \times 10^2$ M^{-1} s^{-1}). Overall, the kinetic results indicate that the CBL 4-chlorobenzoate binding site fails to accommodate the *ortho*- and *meta*-substituted benzoates in an optimal orientation for reaction. Inspection of the CBL structure shown in Figure 1 reveals limited space (~4 Å) between benzoate ring atom C(2), C(3), C(5), or C(6) and the walls of the active site. Thus, whereas CBL productively binds a wide range of benzoates substituted at the *para* position with small hydrophobic substituents, it discriminates against the corresponding *ortho*- and *meta*-substituted benzoates via size exclusion. The *meta*-substituted benzoates are especially challenging substrates. Below, we describe the rational redesign of the CBL 4-chlorobenzoate binding pocket for enhanced activity with 3,4-dichlorobenzoate and 3-chlorobenzoate. Both of these chlorinated benzoates are dead-end byproducts of microbial PCB degradation (*10*). The rational engineering of CBL for thioesterification of 3,4-dichlorobenzoate and 3-chlorobenzoate was carried out to determine whether the 4-chlorobenzoate binding pocket is suitable for redesign to extend substrate range, and to produce novel enzyme catalysts for expanded PCB bioremediation.

Redesign of the CBL 4-Chlorobenzoate Binding Site for Accommodation of a Meta-Chloro Ring Substituent. The CBL substrate specificity profile reported in the previous section shows that the C(4)Cl group makes an important contribution to productive binding. For this reason, 3,4-dichlorobenzoate rather than 3-chlorobenzoate was selected as our first target for CBL engineering. The 3,4-dichlorobenzoate k_{cat}/K_M value of 2×10^3 M^{-1} s^{-1} is 3 orders of magnitude lower than the k_{cat}/K_M value of 4-chlorobenzoate. We can attribute this effect to the *meta*-Cl substituent and specifically to the unfavorable steric effects that may be imposed by this substituent. As indicated in Figure 1, Cδ1

[3] Throughout this paper, changes in the K_M are related to changes in substrate binding affinity. It is well known that only in cases where rapid-equilibrium binding prevails is the K_M equivalent to the dissociation constant of the enzyme−substrate complex. Thus, in this context, we use the change in K_M as an indicator and not as a quantitative measure of the change in binding affinity.

Scheme 2: 4-Chlorobenzoate:CoA Ligase Partial Reactions

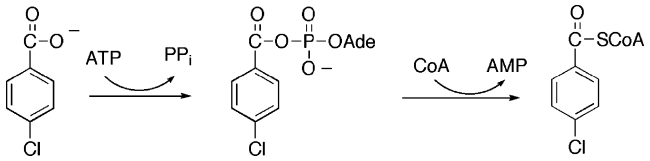

of the Ile303 side chain and Cγ and Cϵ of the Met310 side chain come within close range (~4 Å) of the benzoate ring *meta* carbons. The larger space required for accommodation of *meta*-C(Cl) (1.8 Å C−Cl bond vs 1.1 Å C−H bond) will create steric crowding for both orientations of the bound 3,4-dichlorobenzoate ligand. If additional space can be created by replacement of Ile303 or Met310 with an amino acid having a smaller hydrophobic side chain without disruption of the environment of the reaction center, the catalytic efficiency of CBL toward the 3,4-dichlorobenzoate might be enhanced.

CBL catalysis proceeds via a two-step reaction (Scheme 2) (*43*). The first step involves the nucleophilic displacement of $MgPP_i$ from MgATP by the 4-chlorobenzoate carboxylate to form the 4-chlorobenzoyl adenylate, and the second step involves nucleophilic displacement of AMP from the 4-chlorobenzoyl adenylate by the thiol of CoA to form the 4-chlorobenzoyl-CoA product. The "centers" of these two reactions are thus located outside of the hydrophobic 4-chlorobenzoate binding pocket shown in Figure 1. Therefore, the replacement of Ile303 or Met310 with a small hydrophobic residue should not impair catalysis unless it destabilizes the catalytic scaffold. Ultimately, we chose Ile303 for amino acid replacement because structure-based sequence alignments with other members of the acyl adenylate-forming enzyme superfamily showed that an amino acid as small as Gly is used at this position in some members [for example, the coumarate-CoA ligase from *Arabidopsis thaliana* (*44*), the FadD fatty acyl-CoA synthetase from *E. coli* (*45*), and the long chain fatty acyl-CoA synthetase of *Thermus thermophilus* HB8 (*46*)]. Thus, if the CBL Ile303 residue is replaced with Ala or Gly, it is likely that the stability of the protein, and the arrangement of catalytic residues within the active site, might not be affected. We replaced Ile303 with progressively smaller residues to evaluate the activities of the mutant CBLs toward catalysis of 3,4-dichlorobenzoate CoA thioesterification.

The steady-state kinetic constants of the purified mutants I303V CBL, I303A CBL, and I303G CBL were first measured using 4-chlorobenzoate as a substrate so that we could determine the impact of the mutation on the catalytic efficiency with the native substrate (Table 2; the k_{cat}, K_M and k_{cat}/K_M values measured for ATP and CoA are reported in Table S1 of the Supporting Information). Notably, the 4-chlorobenzoate k_{cat}/K_M decreases with a decrease in the size of the side chain at position 303 in the mutants: I303V CBL, 2.2×10^6 M^{-1} s^{-1} (4.5-fold decrease from the wild-type value); I303A CBL, 6.0×10^5 M^{-1} s^{-1} (16.5-fold decrease from the wild-type value); and I303G CBL, 3.0×10^5 M^{-1} s^{-1} (33-fold decrease from the wild-type value). The decrease in the value of the respective mutants is derived from both a decrease in k_{cat} and an increase in the value of K_M. The k_{cat}/K_M measured for ATP varied but to a smaller degree and not in a trend: wild-type CBL, 9.3×10^4 M^{-1} s^{-1}; I303V CBL, 2.5×10^4 M^{-1} s^{-1} (3.7-fold decrease from the wild-type value); I303A CBL, 3.6×10^4 M^{-1} s^{-1} (2.6-fold decrease from the wild-type value); and I303G CBL 2.2×10^5 M^{-1} s^{-1} (2.4-fold increase from the wild-type value) (Table S1 of the Supporting Information). The k_{cat}/K_M measured for CoA did not vary significantly: wild-type CBL, 3.0×10^4 M^{-1} s^{-1}; I303V CBL, 5.1×10^4 M^{-1} s^{-1} (1.7-fold increase from the wild-type value); I303A CBL, 2.1×10^4 M^{-1} s^{-1} (1.4-fold decrease from the wild-type value); and I303G CBL, 1.6×10^4 M^{-1} s^{-1} (2-fold decrease from the wild-type value). These results show that structural alteration of the 4-chlorobenzoate binding pocket has the greatest impact on the binding and reaction of the carboxylate substrate (vs the binding and activation of ATP and CoA), as one might expect on the basis of the separation of substrate binding sites observed in the CBL structure.

Whereas the binding site of wild-type CBL is expected to be most compatible with 4-chlorobenzoate, the binding sites of the I303V, I303A, and I303G CBL mutants are expected to be most compatible with 3,4-dichlorobenzoate provided that the *meta*-C(Cl) group fills the space vacated by the Ile303 substitution. As reported in Table 2, the k_{cat}/K_M measured with wild-type CBL and 3,4-dichlorobenzoate is 2.0×10^3 M^{-1} s^{-1} and the k_{cat}/K_M value measured for I303V CBL is 2.5×10^4 M^{-1} s^{-1} (12.5-fold increase from the wild-type value), for I303A CBL 1.6×10^5 M^{-1} s^{-1} (80-fold increase from the wild-type value), and for I303G CBL 1.4×10^5 M^{-1} s^{-1} (70-fold increase from the wild-type value). In contrast, the k_{cat} decreased, but only to a comparatively small degree, with decreasing side chain size (wild-type CBL, 0.93 s^{-1}; I303V CBL, 1.8-fold smaller; I303A CBL, 3.4-fold smaller; and I303G CBL, 7.2-fold smaller). The observation that the k_{cat} values measured with the 4-chlorobenzoate substrate and the mutant CBLs are similarly diminished (wild-type CBL, 9.2 s^{-1}; I303V CBL, 3.0-fold smaller; I303A CBL, 6.0-fold smaller; and I303G CBL, 4.6-fold smaller) is indicative of a small perturbation that is not substrate specific.

It is noteworthy that the increase in the k_{cat}/K_M toward the 3,4-dichlorobenzoate substrate caused by the Ile303 substitution is not based on the increase in k_{cat} but rather on the large decrease in the K_M (wild-type CBL, 460 μM; I303V CBL, 23-fold smaller; I303A CBL, 256-fold smaller; and I303G CBL, 495-fold smaller) (Table 2). 3-Bromobenzoate, 3-methylbenzoate, and 3-hydroxybenzoate also displayed increased k_{cat}/K_M values (~10-fold) with the I303A CBL versus wild-type CBAL as a result of a decreased K_M (Table S2 of the Supporting Information). For 3-methoxybenzoate, the increase was only 2-fold. 3-Cyanobenzoate, which did not exhibit detectable substrate activity with wild-type CBL, was discovered to have a k_{cat}/K_M of 1.1×10^2 M^{-1} s^{-1} (Table S2 of the Supporting Information).

We found that the replacement of Ile303 with Tyr or Trp greatly diminishes the catalytic efficiency of 4-chlorobenzoate thioesterification and prevents the 3,4-dichlorobenzoate thioesterification (Table 2). Whereas the K_M for 4-chlorobenzoate was increased ~10000-fold, the K_M values of ATP and CoA were increased by only 2−10-fold (Table S1 of the Supporting Information). Thus, the impact of spatial requirements of the substituted aromatic residues is restricted to 4-chlorobenzoate binding and does not extend to the other substrate binding sites.

Table 2: Steady-State Kinetic Constants k_{cat} and K_M Measured for Wild-Type CBL and I303 CBL Mutants in 50 mM K^+Hepes (pH 7.5 and 25 °C) Containing 15 mM $MgCl_2$, and the Substrates 3.5 mM ATP, 1 mM CoA, and Varying Concentrations of 4-Chlorobenzoate (4-CB), 3-Chlorobenzoate (3-CB), or 3,4-Dichlorobenzoate (3,4-DCB)[a]

	substrate	K_M (μM)	k_{cat} (s^{-1})	k_{cat}/K_M (s^{-1} M^{-1})
wild type	4-CB	$(9.3 \pm 0.9) \times 10^{-1}$	9.2 ± 0.2	9.9×10^6
	3-CB	$(8.0 \pm 0.5) \times 10^2$	$(1.36 \pm 0.02) \times 10^{-1}$	1.7×10^2
	3,4-DCB	$(4.6 \pm 0.1) \times 10^2$	$(9.30 \pm 0.08) \times 10^{-1}$	2.0×10^3
	4-CB	1.4 ± 0.1	3.03 ± 0.06	2.2×10^6
I303V	3-CB	$(5.7 \pm 0.4) \times 10$	$(2.92 \pm 0.07) \times 10^{-2}$	5.1×10^2
	3,4-DCB	$(2.0 \pm 0.2) \times 10$	$(5.2 \pm 0.2) \times 10^{-1}$	2.5×10^4
	4-CB	2.6 ± 0.3	1.54 ± 0.06	6.0×10^5
I303A	3-CB	$(1.25 \pm 0.09) \times 10$	$(1.89 \pm 0.04) \times 10^{-2}$	1.5×10^3
	3,4-DCB	1.8 ± 0.1	$(2.74 \pm 0.06) \times 10^{-1}$	1.6×10^5
	4-CB	6.7 ± 0.7	2.00 ± 0.07	3.0×10^5
I303G	3-CB	9.1 ± 0.3	$(6.49 \pm 0.07) \times 10^{-3}$	7.2×10^2
	3,4-DCB	$(9.3 \pm 0.6) \times 10^{-1}$	$(1.30 \pm 0.03) \times 10^{-1}$	1.4×10^5
	4-CB	$(9 \pm 2) \times 10^2$	$(4.5 \pm 0.4) \times 10^{-1}$	5.0×10^2
I303Y	3-CB		5.5×10^{-5}	
	3,4-DCB	$(1.8 \pm 0.2) \times 10^3$	$(5.8 \pm 0.3) \times 10^{-2}$	3.2
	4-CB	$(1.5 \pm 0.2) \times 10^3$	$(1.9 \pm 0.1) \times 10^{-1}$	1.3×10^2
I303W	3-CB		2.35×10^{-4}	
	3,4-DCB		1.3×10^{-3}	

[a] See Materials and Methods for details. Error limits are derived from the data fitting and not from replicate measurements.

Table 3: Crystallographic and Refinement Data for Crystals of the CBL I303A and I303G Mutant Proteins Complexed with 3-Chlorobenzoate (3-CB) and 3,4-Dichlorobenzoate (3,4-DCB)

	I303G−3-CB	I303G−3,4-DCB	I303A−3-CB	I303A−3,4-DCB
resolution (Å)	30−2.70	30−2.76	30−2.50	30−2.56
space group	$P3_221$	$P3_221$	$P3_221$	$P3_221$
unit cell	$a = b = 127.9$ Å, $c = 71.5$ Å	$a = b = 127.8$ Å, $c = 71.4$ Å	$a = b = 127.9$ Å, $c = 71.4$ Å	$a = b = 128.1$ Å, $c = 71.7$ Å
R_{merge}[a] (%)	4.8 (40.0)	8.8 (52.5)	4.8 (32.0)	5.3 (39.7)
completeness[a] (%)	96.9 (98.9)	99.5 (99.9)	92.8 (100)	90.5 (99.4)
I/σ[a]	15.0 (2.1)	11.5 (1.8)	18.4 (2.2)	12.5 (1.9)
no. of observations	116608	109519	105784	81217
no. of reflections	44023	20899	47472	46521
R_{cryst}[a] (%)	18.8 (32.8)	19.1 (29.5)	19.3 (24.4)	18.5 (28.3)
R_{free}[a] (%)	27.1 (43.4)	25.7 (40.0)	26.6 (35.7)	25.3 (41.7)
Wilson *B*-factor ($Å^2$)	78.0	76.4	64.8	64.5
average *B*-factor (all atoms) ($Å^2$)	47.3	58.0	62.0	56.8
average *B*-factor (N-terminus) ($Å^2$)	47.8	58.2	62.0	56.7
average *B*-factor (C-terminus) ($Å^2$)	44.9	58.0	62.4	57.8
average *B*-factor (solvent) ($Å^2$)	54.2	48.6	59.4	51.5
no. of solvent molecules	31	25	137	107
average *B*-factor (ligand) ($Å^2$)	55.1	53.8	53.3	52.6
rms deviations (lengths, angles)	0.014 Å, 1.59°	0.016 Å, 1.69°	0.013 Å, 1.38°	0.013 Å, 1.43°

[a] Values in parentheses represent statistics for the highest-resolution shell.

We conclude that the hydrophobic CBL 4-chlorobenzoate binding site directs substrate specificity by size exclusion. Moreover, the working hypothesis is that the decrease observed in the 3,4-dichlorobenzoate K_M with the I303V, I303A, and I303G CBL mutants is the direct result of providing a "space" for the *meta*-C(Cl) group.

Determination of the Structure of I303A and I303G CBL Complexed with 3,4-Dichlorobenzoate. The X-ray crystal structures of the I303A and I303G CBL mutants complexed with 3,4-dichlorobenzoate were determined to test our hypothesis. The crystallographic and refinement statistics are presented in Table 3. The electron density maps of the ligand binding sites are shown in Figure 2, and the superposition of the mutant structures with the wild-type CBL−4-chlorobenzoate complex (PDB entry 1T5D) is shown in Figure 3. The structural overlay demonstrates that the mutant proteins adopt a conformation very similar to that of the wild-type CBL enzyme. In particular, the C-terminal domain, which has been observed in multiple orientations for different members of the adenylate-forming family, assumes the same conformation as that of the wild-type enzyme. The rms deviation for Cα atoms is 0.7 Å for all atoms of the N-terminal domain and 1.0 Å for the full-length structures. The C-terminal Ser504 is missing from the structures, which was also found with the wild-type CBAL in complex with 4-chlorobenzoate. In addition, the Gly- and Ser/Thr-rich loop near the active site is disordered. This disorder was also observed in the wild-type CBL structures as well as in the structures of several other members of this enzyme superfamily. A second surface loop (residues 109−112) is also poorly ordered.

The superposition of the residues of the 4-chlorobenzoate binding pocket of the wild-type CBL−4-chlorobenzoate complex and the residues of the 4-chlorobenzoate binding pocket of the I303A CBL(3,4-dichlorobenzoate) complex is shown in stereo in Figure 4A. Within the limits imposed by

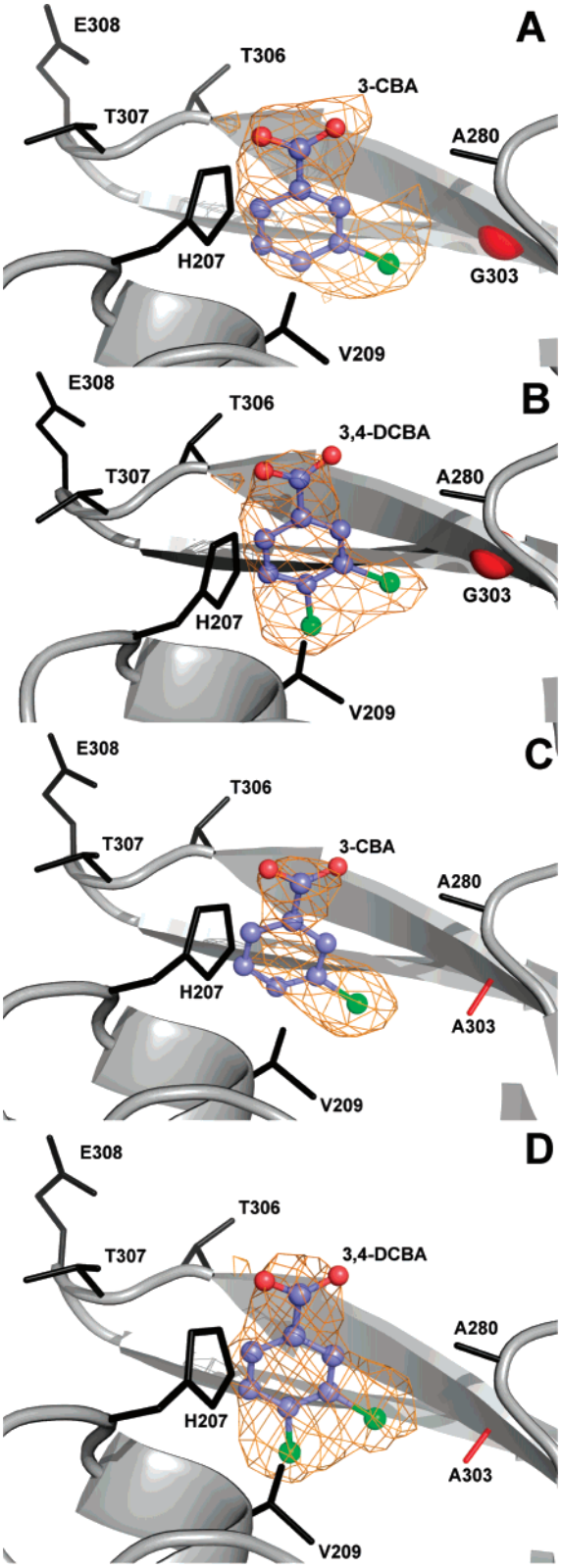

FIGURE 2: Electron density of ligands bound to Ile303 mutants. Unbiased ligand density is shown for (A) 3-chlorobenzoate (3-CB) bound to I303G CBL, (B) 3,4-dichlorobenzoate (3,4-DCB) bound to I303G CBL, (C) 3-chlorobenzoate (3-CB) bound to I303A CBL, and (D) 3,4-dichlorobenzoate (3,4-DCB) bound to I303A CBL. The electron density maps were calculated with coefficients of the form $F_o - F_c$ determined prior to inclusion of the ligand in the refinement. The maps are contoured at 2.5σ. Side chains of neighboring residues are labeled. The mutant residues are colored red. The red sphere in panels A and B represents the Cα position of the CBL Gly303 mutant residue.

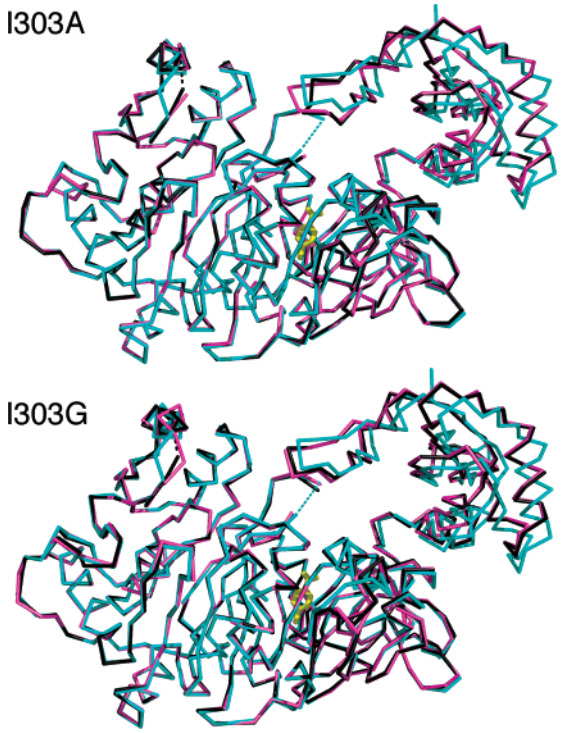

FIGURE 3: Superposition of the main chain carbons of the wild-type CBL structure (1T5D) with the I303A mutant protein structures and the I303G mutants. In both panels, the wild-type structure is colored blue, with the 4-chlorobenzoate ligand shown in yellow stick representation. The mutant proteins are shown bound to 3,4-dichlorobenzoate (black) and bound to 3-chlorobenzoate (pink). The two disordered loops of residues 109−111 and 162−165 are shown with dashed lines. For clarity, only a single ligand is shown in the active site.

the structural resolution (2.2 and 2.6 Å, respectively), the positioning of the binding site residues and the benzoate ligand carboxylate group appears to be unchanged in the mutant complex. Thus, the 3,4-dichlorobenzoate is bound in the correct orientation for reaction in the I303A CBL active site. We also observed that the C(4)Cl group of the 3,4-dichlorobenzoate bound to the I303G CBL mutant fills the C(4)X pocket (see Figure S1A of the Supporting Information). The distance from the C(3)Cl group to the Cβ atom of Ala in the mutant is 3.4 Å. By modeling the 3,4-dichlorobenzoate to fit within the 4-chlorobenzoate binding site of wild-type CBL, and displaying a van der Waals surface on the ligand, we found that a potential steric overlap between the wild-type Ile303 side chain and the C(3)Cl group exists. The distance from the C(3)Cl group to the Cδ1 or Cγ1 atom of Ile303 is only 2.3 Å.

The orientation of 3,4-dichlorobenzoate is such that the C(5)H group is directed at Met310 and the C(3)Cl group is directed at Ala303 (or the Gly of I303G). This orientation is true to the design. To most easily visualize the actual changes in the topology of the binding site that accommodate the ligand in this orientation, VOIDOO (*47*) was used to create a solvent cage (hereafter termed the "ligand cage") that depicts the three-dimensional space available to the ligand. Figure 5A illustrates the accessible ligand cage of the wild-type enzyme. Into this cage we "add back" the 3,4-dichlorobenzoate ligand as it is defined by the I303A CBL-(3,4-dichlorobenzoate) complex structure. The C(3)Cl group extends outside this cage, consistent with the modest catalytic efficiency of the enzyme toward 3,4-dichlorobenzoate (re-

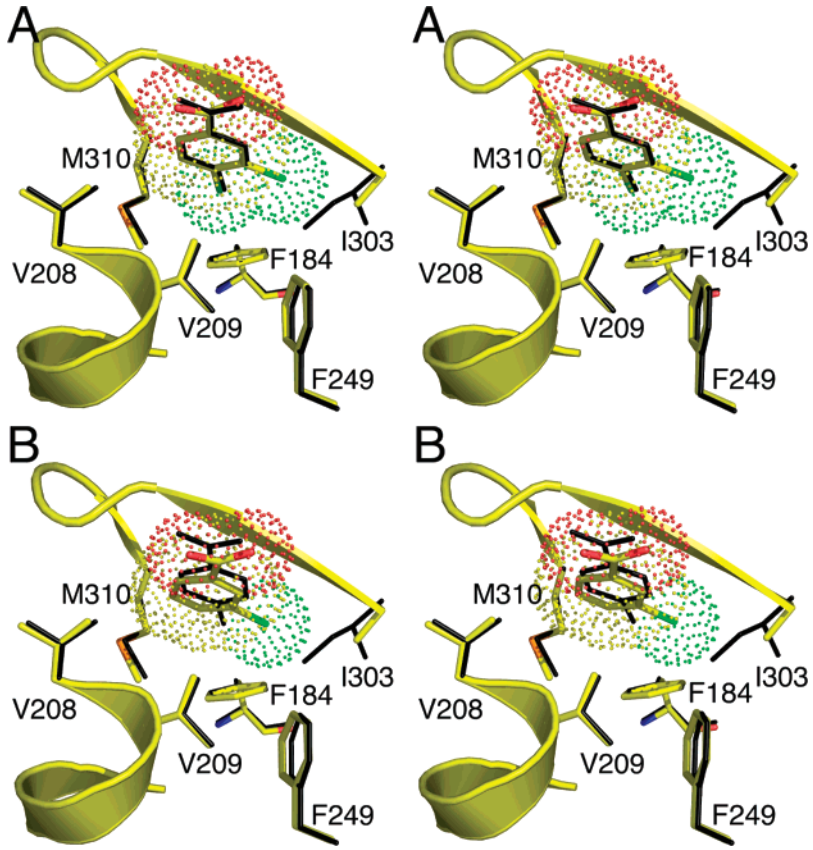

FIGURE 4: Superposition of the wild-type CBL−4-chlorobenzoate complex with the residues of the 4-chorobenzoate binding pocket of the (A) I303A CBL−3,4-dichlorobenzoate complex and (B) I303A CBL−3-chlorobenzoate complex. All protein atoms from the wild-type structure (1T5D) are colored black, while for the mutant structures, carbon atoms are colored yellow, oxygen atoms red, nitrogen atoms blue, sulfur atoms orange, and chloride atoms green. A van der Waals surface is shown on the ligand from the mutant structure.

ported in Table 1). Panels B and C of Figure 5 show the ligand cages of the I303A and I303G CBL mutants generated from the X-ray structures of the I303A and I303G CBL complexes of 3,4-dichlorobenzoate. It is evident from these figures that the 3,4-dichlorobenzoate C(3)Cl group is accommodated within the "extra" space provided by the truncation of I303.

This finding validates the strategy used for the rational redesign of the 4-chlorobenzoate binding pocket for expanded substrate range. The structures show that the needed space was created in the I303 mutants, allowing the enzyme to act on a novel substrate, without a reduction in protein stability or significant impairment of the functioning of the catalytic scaffold. Having achieved this objective, we next sought to engineer the 4-chlorobenzoate binding site so that the requirement for a C(4)Cl group to fill the C(4)X pocket could be eliminated. This work is described in the following section.

Activity Analysis and Determination of the Structure of 3-Dichlorobenzoate Complexes of I303A and I303G CBL Mutants. The low substrate activity observed with benzoate is a clear indication that the C(4)Cl group of the native substrate 4-chlorobenzoate is needed for efficient binding and turnover. On the basis of the X-ray structure of the wild-type CBL−4-chlorobenzoate complex (Figure 1), we surmised that the C(4)Cl group locks the ring in place by filling the C(4)X hydrophobic pocket. 3-Chlorobenzoate has too much steric bulk at C(3) and too little steric bulk at C(4). Indeed, the k_{cat}/K_M value measured with 3-chlorobenzoate and wild-type CBL is quite low, 1.7×10^2 M^{-1} s^{-1} [10000-fold lower than that of 4-chlorobenzoate and 10-fold lower than that of 3,4-dichlorobenzoate (Table 1)]. While the Ala and Gly replacements of I303 increased the 3,4-dichlorobenzoate k_{cat}/K_M value ~100-fold, the 3-chlorobenzoate k_{cat}/K_M value is increased only ~10-fold. The following 3-chlorobenzoate k_{cat}/K_M values were measured for the four mutants: I303V CBL, 5.1×10^2 M^{-1} s^{-1} (3-fold increase from the wild-type value); I303A CBL, 1.5×10^3 M^{-1} s^{-1} (8.8-fold increase from the wild-type value); and I303G CBL, 7.2×10^2 M^{-1} s^{-1} (4.2-fold increase from the wild-type value). The decrease observed in K_M for 3-chlorobenzoate (wild-type CBL, 800 μM; I303V CBL, 14-fold smaller; I303A CBL, 64-fold smaller; and I303G CBL, 88-fold smaller) is partially offset by the decrease in k_{cat} (wild-type CBL, 0.136 s^{-1}; I303V CBL, 4.7-fold smaller; I303A CBL, 7.2-fold smaller; and I303G CBL, 21-fold smaller).

The decreased 3-chlorobenzoate K_M values suggest that increased binding affinity occurs with a decrease in the size of the I303 side chain, consistent with the results obtained with 3,4-dichlorobenzoate. However, the absence of the C(4)-Cl group to fill the C(4)X pocket may lead to nonproductive binding of the 3-chlorobenzoate. To test this hypothesis, the X-ray structures of the I303A and I303G CBL mutants complexed with 3-chlorobenzoate were determined. The electron density maps are shown in Figure 2, and the crystallographic and refinement statistics are presented in Table 3. The only significant difference between these structures and those reported in the previous section for the 3,4-dichlorobenzoate complexes of I303A and I303G CBL is the position of the ligand within the 4-chlorobenzoate

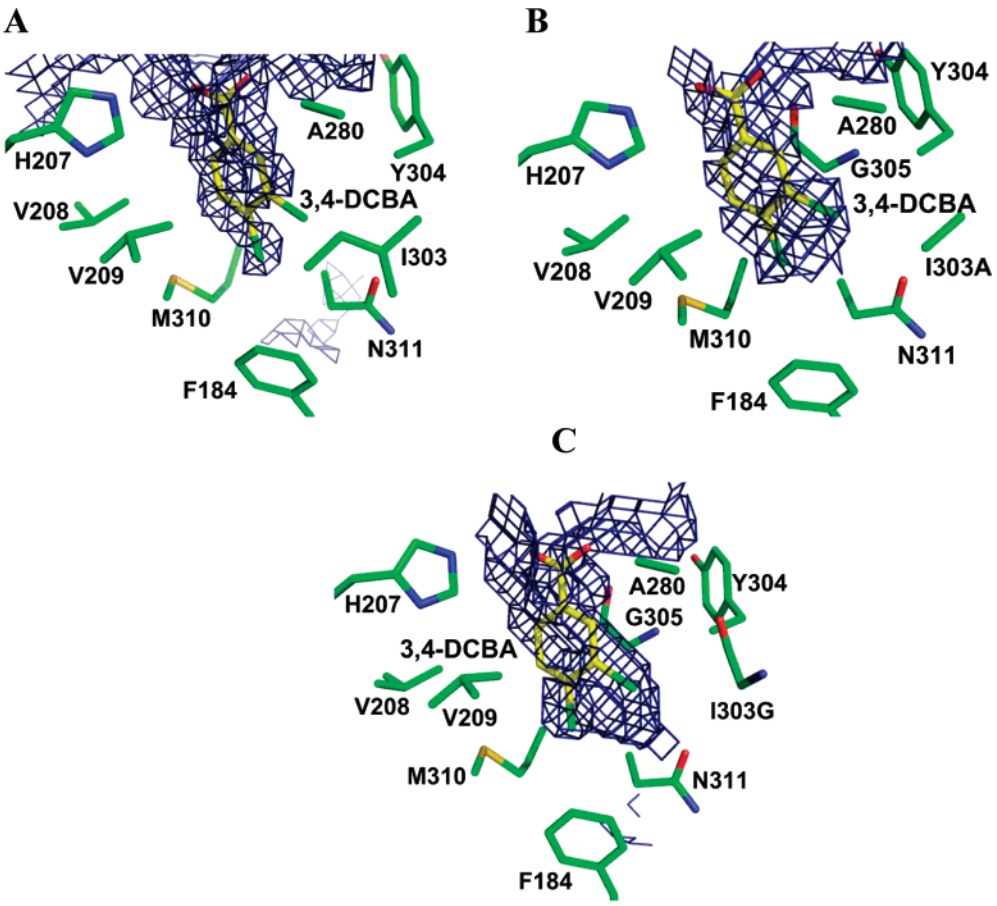

FIGURE 5: (A) Wild-type CBL−4-chlorobenzoate complex (PDB entry 1T5H) with a ligand cage. The 3,4-dichlorobenzoate was modeled in place of the 4-chlorobenzoate. (B) I303A CBL−3,4-dichlorobenzoate complex with a ligand cage. (C) I303G CBL−3,4-dichlorobenzoate complex with a ligand cage. Figures were generated from the X-ray structure coordinates of the respective complexes using VOIDOO (*47*).

binding pocket. Figure 4B shows the superposition of the wild-type enzyme and the I303A mutant bound to 3-chlorobenzoate. A superposition of the wild-type enzyme with the I303G mutant is shown in Figure S1 of the Supporting Information. It is evident from these structures that the 3-chlorobenzoate ligand is positioned too deep within the 4-chlorobenzoate binding pocket. We concluded that this is because the C(4)H group is not able to adequately fill the C(4)X pocket which is needed to lock the ring in a productive binding orientation. In both mutants, the 3-chlorobenzoate carboxylate group is positioned 0.7 Å below the position of the carboxylate group of the 3,4-dichlorobenzoate or the 4-chlorobenzoate carboxylate group observed in the wild-type CBL(4-chlorobenzoate) complex.

Design of CBL Variants with Improved 3-Chlorobenzoate Conversion Rates. To increase CBL activity with 3-chlorobenzoate, we carried out site-directed mutagenesis, replacing the residues that form the C(4)X binding pocket with larger amino acids. Residues Phe184, Asn311, and Met310 were identified as the nearest neighbors to the substrate C(4)-Cl group (Figure 1). The I303A CBL mutant was used as the starting point for the C(4)X pocket engineering. Phe184, Asn311, and Met310 were separately replaced with amino acids having slightly greater steric bulk (see the list of mutants tested in Table 4). The use of "natural" amino acids placed a severe limitation on the remodeling. Nevertheless, in silico models generated for the planned mutants suggested that a small yet possibly significant decrease in the size of the C(4)X pocket might be achieved. At this stage, we are most interested in proof of concept. In particular, the issue to be addressed is whether the plasticity of the site is sufficient to adapt to the steric and electrostatic perturbations introduced by the restructuring of the C(4)X pocket.

For the 3-chlorobenzoate thioesterification catalyzed by F184W/I303A CBL, the $k_{cat}/K_M = 5.4 \times 10^3$ M^{-1} s^{-1} (Table 4). This represents a 32-fold increase in efficiency relative to that of wild-type CBL and a 4-fold increase relative to that of the I303A CBL mutant. In contrast, the $k_{cat}/K_M = 2.3 \times 10^2$ M^{-1} s^{-1} measured with 3-chlorobenzoate and F184Y/I303A CBL is 6.5-fold smaller than that measured for I303A CBL. The K_M values measured for ATP and CoA (Table S4 of the Supporting Information) for these two mutants (and the mutants described below) are not significantly different from those measured with wild-type CBL. Thus, the impact of the amino acid substitutions appears to be limited to the 4-chlorobenzoate binding site.

Next, CBL M310 and N311 mutants were examined. Unfortunately, only the N311Q/I303A mutant exhibited enhanced enzyme catalytic activity relative to the I303A single mutation (Table 4). The k_{cat}/K_M measured with 3-chlorobenzoate and N311Q/I303A CBAL is 3.6×10^3 M^{-1} s^{-1} which corresponds to a 2.4-fold increase from that of I303A. This is largely a K_M effect. The k_{cat}/K_M values measured for N311H/I303A and N311T/I303A are smaller than that of I303A (19- and 2-fold, respectively). Although the k_{cat} values of these two N311 double mutants are increased over that of I303A CBL (1.4-fold increase with N311H/I303A and 12-fold increase with N311T/I303A), the

Table 4: Steady-State Kinetic Constants Measured for Wild-Type CBL and CBL Mutant Catalysis of 3-Chlorobenzoate Thioesterification in Reaction Solutions Containing 3.5 mM ATP, 1 mM CoA, 15 mM $MgCl_2$, and 50 mM K^+Hepes (pH 7.5 and 25 °C)[a]

	K_M (μM)	k_{cat} (s^{-1})	k_{cat}/K_M (s^{-1} M^{-1})
wild type	$(8.0 \pm 0.5) \times 10^2$	$(1.36 \pm 0.02) \times 10^{-1}$	1.7×10^2
I303A	$(1.25 \pm 0.09) \times 10$	$(1.89 \pm 0.04) \times 10^{-2}$	1.5×10^3
N311H/I303A	$(3.35 \pm 0.05) \times 10^2$	$(2.64 \pm 0.01) \times 10^{-2}$	7.9×10
N311Q/I303A	5.9 ± 0.3	$(2.15 \pm 0.03) \times 10^{-2}$	3.6×10^3
N311T/I303A	$(3.1 \pm 0.3) \times 10^2$	$(2.19 \pm 0.07) \times 10^{-1}$	7.1×10^2
F184W/I303A	$(1.40 \pm 0.7) \times 10$	$(7.5 \pm 0.1) \times 10^{-2}$	5.4×10^3
F184Y/I303A	$(2.3 \pm 0.1) \times 10$	$(5.39 \pm 0.06) \times 10^{-3}$	2.3×10^2
F184W/I303A/N311Q	7.2 ± 0.8	$(3.2 \pm 0.1) \times 10^{-2}$	4.4×10^3
M310L/I303A	ND[b]	2.0×10^{-3}	ND[b]
M310I/I303A	ND[b]	7.8×10^{-3}	ND[b]
V209Y/I303A	ND[b]	2.1×10^{-3}	ND[b]
V209W/I303A	ND[b]	1.7×10^{-3}	ND[b]
V209T/I303A	$(3.0 \pm 0.2) \times 10$	$(7.1 \pm 0.2) \times 10^{-2}$	2.4×10^3
V208Q/I303A	$(2.0 \pm 0.3) \times 10^2$	$(1.65 \pm 0.05) \times 10^{-3}$	8.3
F184W/I303A/V209T	11.1 ± 0.8	$(1.01 \pm 0.01) \times 10^{-1}$	9.1×10^3

[a] See Materials and Methods for details. Error limits are derived from the data fitting and not from replicate measurements. [b] Not determined.

increased K_M values (27- and 25-fold, respectively) counter the k_{cat} effect. Last, the triple mutant F184W/N311Q/I303A was prepared to determine whether these three site mutations would have an additive effect on catalytic efficiency. The triple mutant is more active than the double mutant N311Q/I303A but not as active as the double mutant F184W/I303A.

The CBL mutants V209Y/I303A and V209W/I303A are not active with 3-chlorobenzoate (Table 4). In contrast, V209T/I303A CBL displayed a k_{cat} of 0.071 s^{-1}, 3.8-fold larger than the k_{cat} of I303A. However, the K_M is also increased. The CBL triple mutant F184W/I303A/V209T on the other hand exhibited a k_{cat}/K_M of 9.1×10^3 M^{-1} s^{-1} with 3-chlorobenzoate. This represents a 54-fold increase over the k_{cat}/K_M of wild-type CBL. The F184W/I303A/N311Q mutant displayed a k_{cat}/K_M of 4.0×10^3 M^{-1} s^{-1} with 3-chlorobenzoate (27-fold increase over the wild-type value).

The F184W/I303A/V209T CBL mutant is the most active mutant with 3-chlorobenzoate serving as the substrate. However, compared to I303A CBL which was used as the starting point for engineering the C(4)Cl pocket, F184W/I303A/V209T CBL is only 6-fold more active. Thus, the replacement of the pocket residues with residues achieved the desired affect, but overall, the observed rate enhancement is modest. This suggests that the positions of the main chain segments that frame the C(4)Cl pocket should be targeted for engineering a closed pocket. In future work, this alternative will be explored.

Summary and Conclusion. These studies show that the 4-chlorobenzoate binding site has evolved to function within the 4-chlorobenzoate pathway (Scheme 1). The high k_{cat}/K_M for 4-chlorobenzoate contrasted with the low k_{cat}/K_M for the pathway product 4-hydroxybenzoate, evidence an effective mechanism for substrate discrimination. The substrate specificity profile analyzed in the context of the CBL(4-chlorobenzoate) structure suggested that the substrate binding affinity and the orientation of the substrate carboxylate group for reaction are controlled by two distinct properties of the binding pocket. One property is hydrophobicity, and the other is "lock-in-key" topological complementation. The addition of nonpolar ring substituents at the *ortho* or *meta* positions of the substrate is not well-tolerated because of the steric hindrance that taxes binding affinity. The substitution of the *para*-C(Cl) group with substituents similar in size and hydrophobicity is well-tolerated because these substituents are able to fill the *para*-C(Cl) subpocket at the bottom of the binding site and by doing so lock the ring in the correct position for alignment of the carboxylate group for attack at the α-P atom of the bound ATP (Scheme 2).

In contrast, benzoates that do not possess a C(4) substituent of adequate size will "sink" into the pocket and the ring carboxylate will be poorly oriented for reaction. The replacement of the 4-chlorobenzoate binding pocket residue Ile303 with Ala created adequate space for the accommodation of the C(3)Cl group (*meta*) of the 3,4-dichlorobenzoate and increased the k_{cat}/K_M from 2.0×10^3 to 1.6×10^5 M^{-1} s^{-1}. The attempted reconstruction of the CBL C(4)Cl subpocket to prop the 3-chlorobenzoate within the binding site of the I303A CBL mutant was only modestly successful because of the limitation of the structural changes that could be made at this site using natural amino acids. It is likely that substitutions made at the second sphere of binding site residues via focused random mutagenesis (*30*, *34*) could be employed to further constrict the C(4) pocket for optimized activity with 3-chlorobenzoate.

Overall, this work shows that CBL has excellent potential as a catalytic platform for the rational design of CoA thioesterification catalysts for use in activation of aromatic acids for bioremediation applications. Moreover, in a recent publication, Smith and co-workers (*48*) reported that a Trp to Gly replacement within the acetate binding site in acetyl-CoA synthetase switches the preference for acetate to a preference for valerate. Thus, the acyl adenylate-forming enzyme superfamily may serve as a rich source of designer catalysts for the synthesis of acyl-CoA thioesters. For those family members that participate in nonribosomal peptide antibiotic synthetic pathways (*49*−*51*), engineering substrate specificity may lead to the development of novel antibiotics.

SUPPORTING INFORMATION AVAILABLE

Tables of steady-state kinetic constants and a figure of I303G CBL ligand complexes. This material is available free of charge via the Internet at http://pubs.acs.org.

REFERENCES

1. De Voogt, P., Wells, D. E., Reutergardh, L., and Brinkman, U. (1990) Biological activity, determination, and occurrence of planar, mono- and di-ortho PCBs, *Int. J. Anal. Chem. 40*, 1−46.

2. Safe, S. (1992) Toxicology, structure-function relationship, and human and environmental health impacts of polychlorinated biphenyls: Progress and problem, *Environ. Health Perspect. 100*, 259−268.
3. Faroon, O., Jones, D., and de Rosa, C. (2001) Effects of polychlorinated biphenyls on the nervous system, *Toxicol. Ind. Health 16*, 305−333.
4. Aoki, Y. (2001) Polychlorinated biphenyls, polychlorinated dibenzo-p-dioxins, and polychlorinated dibenzofurans as endocrine disrupters: What we have learned from Yusho disease, *Environ. Res. 86*, 2−11.
5. Faroon, O. M., Keith, S., Jones, D., and De Rosa, C. (2001) Carcinogenic effects of polychlorinated biphenyls, *Toxicol. Ind. Health 17*, 41−62.
6. Faroon, O. M., Keith, L. S., Williams, M., Murray, H. E., Jones, D. E., and De Rosa, C. T. (2004) Comments on "Potential human cancer risks from exposure to PCBs: A tale of two evaluations", *Crit. Rev. Toxicol. 34*, 499−501; author reply 503−505.
7. Guo, Y. L., Lambert, G. H., Hsu, C. C., and Hsu, M. M. (2004) Yucheng: Health effects of prenatal exposure to polychlorinated biphenyls and dibenzofurans, *Int. Arch. Occup. Environ. Health 77*, 153−158.
8. Haggblom, M. M. (1992) Microbial breakdown of halogenated aromatic pesticides and related compounds, *FEMS Microbiol. Rev. 9*, 29−71.
9. Higson, F. K. (1992) Microbial degradation of biphenyl and its derivatives, *Adv. Appl. Microbiol. 37*, 135−164.
10. Pieper, D. H. (2005) Aerobic degradation of polychlorinated biphenyls, *Appl. Microbiol. Biotechnol. 67*, 170−191.
11. Rodrigues, J. L., Kachel, C. A., Aiello, M. R., Quensen, J. F., Maltseva, O. V., Tsoi, T. V., and Tiedje, J. M. (2006) Degradation of aroclor 1242 dechlorination products in sediments by *Burkholderia xenovorans* LB400(ohb) and *Rhodococcus* sp. strain RHA1-(fcb), *Appl. Environ. Microbiol. 72*, 2476−2482.
12. Nishi, A., Tominaga, K., and Furukawa, K. (2000) A 90-kilobase conjugative chromosomal element coding for biphenyl and salicylate catabolism in *Pseudomonas putida* KF715, *J. Bacteriol. 182*, 1949−1955.
13. Toussaint, A., Merlin, C., Monchy, S., Benotmane, M. A., Leplae, R., Mergeay, M., and Springael, D. (2003) The biphenyl- and 4-chlorobiphenyl-catabolic transposon Tn4371, a member of a new family of genomic islands related to IncP and Ti plasmids, *Appl. Environ. Microbiol. 69*, 4837−4845.
14. Furukawa, K., and Miyazaki, T. (1986) Cloning of a gene cluster encoding biphenyl and chlorobiphenyl degradation in *Pseudomonas pseudoalcaligenes*, *J. Bacteriol. 166*, 392−398.
15. Hayase, N., Taira, K., and Furukawa, K. (1990) *Pseudomonas putida* KF715 bphABCD operon encoding biphenyl and polychlorinated biphenyl degradation: Cloning, analysis, and expression in soil bacteria, *J. Bacteriol. 172*, 1160−1164.
16. Kosono, S., Maeda, M., Fuji, F., Arai, H., and Kudo, T. (1997) Three of the seven bphC genes of *Rhodococcus erythropolis* TA421, isolated from a termite ecosystem, are located on an indigenous plasmid associated with biphenyl degradation, *Appl. Environ. Microbiol. 63*, 3282−3285.
17. Masai, E., Sugiyama, K., Iwashita, N., Shimizu, S., Hauschild, J. E., Hatta, T., Kimbara, K., Yano, K., and Fukuda, M. (1997) The bphDEF meta-cleavage pathway genes involved in biphenyl/polychlorinated biphenyl degradation are located on a linear plasmid and separated from the initial bphACB genes in *Rhodococcus* sp. strain RHA1, *Gene 187*, 141−149.
18. Kong, H. L., and Sayler, G. S. (1983) Degradation and total mineralization of monohalogenated biphenyls in natural sediment and mixed bacterial culture, *Appl. Environ. Microbiol. 46*, 666−672.
19. Layton, A. C., Sanseverino, J., Wallace, W., Corcoran, C., and Sayler, G. S. (1992) Evidence for 4-chlorobenzoic acid dehalogenation mediated by plasmids related to pSS50, *Appl. Environ. Microbiol. 58*, 399−402.
20. Su-Yuan Lai, W.-h. Z., Wu, R., Wei, Y., Lu, X., Layton, A. C., Sayler, G. S., and Dunaway-Mariano, D. (2007) The Plasmid pSS70 Encoded 4-Chlorobenzoate Pathway of the 4-Chlorinated Biphenyl-Degrader *Alcaligenes* sp. Strain ALP83# (submitted for publication).
21. Lai, S.-Y. (1996) Characterization of the genes encoding the enzymes of the 4-chlorobenzoate degradation pathway in *Alcaligenes* sp. strain AL3007, Ph.D. Thesis, University of Maryland, College Park, MD.
22. Dunaway-Mariano, D., and Babbitt, P. C. (1994) On the origins and functions of the enzymes of the 4-chlorobenzoate to 4-hydroxybenzoate converting pathway, *Biodegradation 5*, 259−276.
23. Ismail, W., El-Said Mohamed, M., Wanner, B. L., Datsenko, K. A., Eisenreich, W., Rohdich, F., Bacher, A., and Fuchs, G. (2003) Functional genomics by NMR spectroscopy. Phenylacetate catabolism in *Escherichia coli*, *Eur. J. Biochem. 270*, 3047−3054.
24. Gescher, J., Eisenreich, W., Worth, J., Bacher, A., and Fuchs, G. (2005) Aerobic benzoyl-CoA catabolic pathway in *Azoarcus evansii*: Studies on the non-oxygenolytic ring cleavage enzyme, *Mol. Microbiol. 56*, 1586−1600.
25. Merkel, S. M., Eberhard, A. E., Gibson, J., and Harwood, C. S. (1989) Involvement of coenzyme A thioesters in anaerobic metabolism of 4-hydroxybenzoate by *Rhodopseudomonas palustris*, *J. Bacteriol. 171*, 1−7.
26. Chang, K. H., Liang, P. H., Beck, W., Scholten, J. D., and Dunaway-Mariano, D. (1992) Isolation and characterization of the three polypeptide components of 4-chlorobenzoate dehalogenase from *Pseudomonas* sp. strain CBS-3, *Biochemistry 31*, 5605−5610.
27. Gulick, A. M., Lu, X., and Dunaway-Mariano, D. (2004) Crystal structure of 4-chlorobenzoate:CoA ligase/synthetase in the unliganded and aryl substrate-bound states, *Biochemistry 43*, 8670−8679.
28. Vopel, S., Muhlbach, H., and Skerra, A. (2005) Rational engineering of a fluorescein-binding anticalin for improved ligand affinity, *Biol. Chem. 386*, 1097−1104.
29. Ema, T., Fujii, T., Ozaki, M., Korenaga, T., and Sakai, T. (2005) Rational control of enantioselectivity of lipase by site-directed mutagenesis based on the mechanism, *Chem. Commun.*, 4650−4651.
30. Chica, R. A., Doucet, N., and Pelletier, J. N. (2005) Semi-rational approaches to engineering enzyme activity: Combining the benefits of directed evolution and rational design, *Curr. Opin. Biotechnol. 16*, 378−384.
31. Magnusson, A. O., Takwa, M., Hamberg, A., and Hult, K. (2005) An S-selective lipase was created by rational redesign and the enantioselectivity increased with temperature, *Angew. Chem., Int. Ed. 44*, 4582−4585.
32. Magnusson, A. O., Rotticci-Mulder, J. C., Santagostino, A., and Hult, K. (2005) Creating space for large secondary alcohols by rational redesign of *Candida antarctica* lipase B, *ChemBioChem 6*, 1051−1056.
33. Antikainen, N. M., and Martin, S. F. (2005) Altering protein specificity: Techniques and applications, *Bioorg. Med. Chem. 13*, 2701−2716.
34. Leisola, M., and Turunen, O. (2007) Protein engineering: Opportunities and challenges, *Appl. Microbiol. Biotechnol. 75*, 1225−1232.
35. Nowlan, C., Li, Y., Hermann, J. C., Evans, T., Carpenter, J., Ghanem, E., Shoichet, B. K., and Raushel, F. M. (2006) Resolution of chiral phosphate, phosphonate, and phosphinate esters by an enantioselective enzyme library, *J. Am. Chem. Soc. 128*, 15892−15902.
36. Bradford, M. M. (1976) A rapid and sensitive method for the quantitation of microgram quantities of protein utilizing the principle of protein-dye binding, *Anal. Biochem. 72*, 248−254.
37. Gulick, A. M., Horswill, A. R., Thoden, J. B., Escalante-Semerena, J. C., and Rayment, I. (2002) Pentaerythritol propoxylate: A new crystallization agent and cryoprotectant induces crystal growth of 2-methylcitrate dehydratase, *Acta Crystallogr. D58*, 306−309.
38. Otwinowski, Z. M., and Minor, W. (1997) Processing of X-ray Diffraction Data Collected in Oscillation Mode, *Methods Enzymol. 276*, 307−326.
39. Vagin, A., and Teplyakov, A. (1997) MOLREP: An automated program for molecular replacement, *J. Appl. Crystallogr. 30*, 1022−1025.
40. Murshudov, G. N., Vagin, A. A., and Dodson, E. J. (1997) Refinement of macromolecular structures by the maximum-likelihood method, *Acta Crystallogr. D53*, 240−255.
41. Emsley, P., and Cowtan, K. (2004) Coot: Model-building tools for molecular graphics, *Acta Crystallogr. D60*, 2126−2132.
42. Winn, M. D., Isupov, M. N., and Murshudov, G. N. (2001) Use of TLS parameters to model anisotropic displacements in macromolecular refinement, *Acta Crystallogr. D57*, 122−133.
43. Chang, K. H., and Dunaway-Mariano, D. (1996) Determination of the chemical pathway for 4-chlorobenzoate:coenzyme A ligase catalysis, *Biochemistry 35*, 13478−13484.

44. Schneider, K., Hovel, K., Witzel, K., Hamberger, B., Schomburg, D., Kombrink, E., and Stuible, H. P. (2003) The substrate specificity-determining amino acid code of 4-coumarate:CoA ligase, *Proc. Natl. Acad. Sci. U.S.A. 100*, 8601−8606.
45. Black, P. N., DiRusso, C. C., Metzger, A. K., and Heimert, T. L. (1992) Cloning, sequencing, and expression of the fadD gene of *Escherichia coli* encoding acyl coenzyme A synthetase, *J. Biol. Chem. 267*, 25513−25520.
46. Hisanaga, Y., Ago, H., Nakagawa, N., Hamada, K., Ida, K., Yamamoto, M., Hori, T., Arii, Y., Sugahara, M., Kuramitsu, S., Yokoyama, S., and Miyano, M. (2004) Structural basis of the substrate-specific two-step catalysis of long chain fatty acyl-CoA synthetase dimer, *J. Biol. Chem. 279*, 31717−31726.
47. Kleywegt, G. J., and Jones, T. A. (1994) Detection, delineation, measurement and display of cavities in macromolecular structures, *Acta Crystallogr. D50*, 178−185.
48. Ingram-Smith, C., Woods, B. I., and Smith, K. S. (2006) Characterization of the acyl substrate binding pocket of acetyl-CoA synthetase, *Biochemistry 45*, 11482−11490.
49. Stachelhaus, T., Mootz, H. D., and Marahiel, M. A. (1999) The specificity-conferring code of adenylation domains in nonribosomal peptide synthetases, *Chem. Biol. 6*, 493−505.
50. Eppelmann, K., Stachelhaus, T., and Marahiel, M. A. (2002) Exploitation of the selectivity-conferring code of nonribosomal peptide synthetases for the rational design of novel peptide antibiotics, *Biochemistry 41*, 9718−9726.
51. Grunewald, J., and Marahiel, M. A. (2006) Chemoenzymatic and template-directed synthesis of bioactive macrocyclic peptides, *Microbiol. Mol. Biol. Rev. 70*, 121−146.

BI701609W